ON OCCUPANT IDENTIFICATION AND RELATED CRASH OUTCOME IN OUT OF POSITION CONDITIONS

ALBERTO VERGNANO[1], JAN KOVANDA[2]

[1]Enzo Ferrari Department of Engineering , University of Modena and Reggio Emilia, Modena, Italy

[2]Faculty of Mechanical Engineering, University of West Bohemia, Pilsen, Czech Republic

DOI: 10.17973/MMSJ.2025_03_2025001

alberto.vergnano@unimore.it

The methodology for crash tests in vehicle development and homologation is based on dummies sitting in a standardized posture, defined by the H-point of the car body and design specifications. As a result, injury criteria are directly influenced by these precisely defined initial conditions. Out-of-Position scenarios are not included in passive safety tests but are usually analysed conventionally through specialized experiments. The combination of crash dynamics and improper airbag deployment can increase the forces exerted on the body. While airbags have saved numerous lives, statistics also report injuries and fatalities caused by improper contact with deploying airbags. This study examines strategies to make the Airbag Control Unit effectively adaptive to an occupant position. Pre-crash scenarios are identified using sensors in the vehicle seat and the corresponding outcomes are simulated. The research highlights the importance of a thorough examination of crash circumstances, process and outcomes to improve safety in intelligent vehicles.

CAR SEAT, INTELLIGENT VEHICLE, SAFETY SYSTEM, DRIVING EXPERIMENT, OUT-OF-POSITION, CRASH TEST, DRIVER MONITORING

1 INTRODUCTION

The epidemic of road accidents caused by the increasing number of vehicles on the roads is still largely unsolved by modern society. Each year, more than 1.2 million people worldwide lose their lives in car accidents, while hundreds of thousands more are injured, with some sustaining lifelong disabilities [Wismans 2020]. Therefore, it is crucial to incorporate advanced active and passive safety systems into vehicle design to minimize the number of car accidents and reduce the outcome of unavoidable crashes.

In the event of a road accident, a sensor system triggers the deployment of the airbags in the car cockpit to mitigate the impact and reduce potential injuries. However, airbag deployment is not unconditionally beneficial. Research has extensively documented that deployment against an Out of Position (OP) occupant may result in serious injuries rather than reducing the effects of a crash [Maxeiner 1997; Potula 2012 ; Yoganandan 2007]. While this drawback must be reduced in traditional vehicles [FMVSS 2016a; FMVSS 2016b; Lund 2003], where it is still considered a misuse condition, it needs to be definitively overcome in Level 4 (High Automation) and Level 5 (Full Automation) vehicles [SAE 2014], where occupants will increasingly be allowed to engage in non-driving activities, including assuming unconventional postures. The development of future intelligent vehicles should prioritize technologies for the active integration of human passengers on board.

The Airbag Control Unit (ACU) can already adjust the deployment to the speed, impact severity, seatbelt usage, and body size [Farmer 2007; Mon 2007; Yang, 1996]. To make the ACU effectively adaptive, the circumstances, the process, and the results of accidents must be carefully identified using as many elements as possible. Although the crash conditions are reproduced by probability variables, the deterministic view is still dominant in them. Stochastic views and statistics-evaluations concern accidents which have already happened. The typical, most frequently happening crash situations are taken from the above-mentioned after-crash statistics. The exact data can be determined by the pre-crash initial conditions and one of them is the current seating geometry of vehicle occupants. The crash tests run on the base on the exactly sitting position, the reality can be different. Inside scenario, including pre-crash conditions, can be monitored by artificial vision systems [Bergasa 2006; Borghi 2018; Dong 2010]. However, cameras may struggle to accurately detect the body of occupants who are in an OP.

The aim of this paper is to present how the seating conditions of the occupants can be identified by sensorized seats [Federspiel 2004; Schousek 1995; White 1991] and what physical outcome these circumstances lead to. Four prototypes of sensorized have been developed in this research and tested in dynamic experiments with many drivers, unlike almost all other works in literature. The position conditions identified by these prototypes of sensorized seat are discussed in the present paper from the airbag interaction point of view.

The paper is organized as follows. Section 2 highlights the crash scenario to be investigated, followed by Sec. 3 introducing the seat prototypes for occupant monitoring. Section 4 presents the experiments with the prototypes. Section 5 investigates the airbag interaction with a test dummy while Sec. 6 draws the concluding remarks.

2 PASSIVE SAFETY OF VEHICLES, CRASH CONDITIONS

In a crash situation, the yield strength of the involved parts' material is surpassed, and sometimes even their ultimate strength limits are reached accompanied by total failure of the component [Talarico 2012]. Plastic deformation of the impacted parts following primary elastic deflection occurs. Plastic deformation energy takes then over practically all kinetic energy of the impacting bodies.

Despite real-world car crashes and impacts have an infinite number of varieties, the impact scenarios used for car design are assumed from legal requirements and consumer tests. The crash severity depends on the total kinetic energy of both impacting bodies. Any car body can protect the passengers to some degree, which is agreed by the legislators and public for the time being and expressed in international regulations, prescriptions of public organizations and factory rules.

General demands posed on the carbody during and after a crash can be briefly summarized as follows [Talarico 2012]:

- maximum strength of the passenger compartment is demanded; the interior space of the passenger compartment should stay as intact as possible; relative movement of steering assembly towards body must be kept in tolerable limits; seats must not get loose; penetration of sharp corners into the passenger compartment during the crash must be completely avoided even in most severe crashes; the volume necessary for survival of any passenger must be preserved even in most severe

crashes; luggage in the luggage compartment must not enter the passenger compartment;
- the possibility to open at least two doors must be preserved;
- optimized force/deformation characteristics of the crash zones are demanded; mean as well as maximum translational and rotational decelerations of the car-body at passengers´ seats during the crash should be minimized;
- mean values as well as maximum decelerations and forces acting on prescribed occupants´ body parts (head, thorax, hips, etc.) should be minimized; in tests, they are evaluated accordingly to prescribed criterions of injury rates; seat belts, airbags and other retention means, upholstery, etc. play here deciding role.

The last two requirements are strongly linked with the body dynamics during crash, i.e. with initial sitting geometry, which is prescribed in advance in the test conditions. Most tests are carried out with test dummies of very sophisticated design, which can show the injury risks of different body parts. Injury criteria, which form a vital part of the evaluation of passive safety in different tests, are the critical parameters for the results of approval tests. To get in all criteria bellow the predefined threshold is a difficult indirect engineering task, which requires deep knowledge, many experiments and simulations.

The airbag is critical element from sitting geometry point of view. Its design is based on standard speed crashes, regulated in national and company tests. Passive safety is directly governed by regulations and prescriptions, differing in Europe [EU 2024], USA [FMVSS 2016a; FMVSS 2016b] and Japan [JASIC 2021]. On the other hand, private organizations, such as NCAP [Euro Ncap 2024), are proposing steadily harder test conditions, which will have a further impact on the car body design.

3 PROTOTYPES OF SENSORIZED SEATS

The layout, construction and operating principles of four prototype seats are presented hereafter.

3.1 *Pressure Sensors Embedded in a Vehicle Seat*

The first prototype is designed with a number of sensors spread below its surface. Thin Force Sensing Resistors (FSR) are used to monitor the contact pressure [Yaniger 1991]. Based on the specifications provided in [Gyi 1998], the seat cover is equipped with 16 FSR 402 [Interlink Electronics 2024], with a 0.45 mm thickness and a 13 mm diameter active surface. The sensors, depicted in Fig. 1a, are arranged as shown in Fig. 1b, with labels in the controller software corresponding to the initials of Seat, Backrest, Left, and Right.

In real dynamic driving conditions, the pressure field continuously changes due to the balancing of body inertia in response to vehicle accelerations during speeding up, braking, or turning, as well as the occupant's movement on the seat. To monitor the occupant's movement only, the effect of vehicle dynamics on pressure field variations must be cancelled out in the methodology. A BNO055 IMU [Bosch 2024] is used to monitor the vehicle as a moving platform [Chakravarty 2013; Vlahogianni 2017]. The BNO055 is a 9-axis absolute orientation sensor that integrates a triaxial accelerometer, a triaxial gyroscope, and a triaxial geomagnetic sensor.

The 16 FSRs and the BNO055 are integrated via an Arduino Mega 2560 microcontroller [Arduino 2024]. The first calibration routine aligns the BNO055 reference system with the vehicle one.

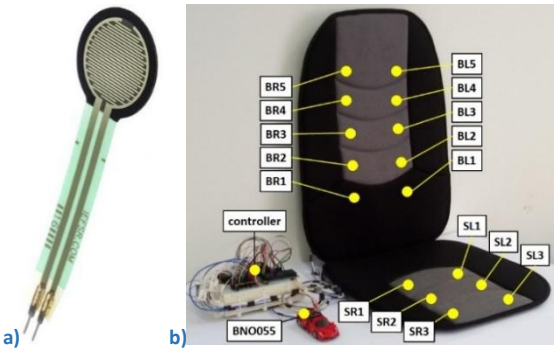

Figure 1. Sensor system: a) FSR and b) layout with FSRs, IMU and controller [Vergnano 2020b].

In the experiments, individual sensors do not provide meaningful information on their own. To extract useful data regarding the occupant position, the sensors must be grouped to compute overall values. The FSRs are organized based on their location as Seat (S) (sensors SR1, SR2, SR3, SL1, SL2, and SL3), Backrest (B) (sensors BR1 to BR5 and BL1 to BL5), or Seat+Backrest (SB) (all sensors combined). As the first evaluation step, the signal values in the S, B, and SB groups are Averaged (A), resulting in A_S, A_B and A_{SB} cumulative values. Next, for each group, the Pressure Center (PC) in the longitudinal x and transversal y directions is defined as:

$$PC_{x,j} = \sum_{i=1}^{n} c_{x,i,j} FSR_i \approx acc_x$$
$$PC_{y,j} = \sum_{i=1}^{n} c_{y,i,j} FSR_i \approx acc_y \quad (1)$$

where FSR_i is the *i* signal value, the *j* subscript is S, B or SB for the different evaluations on the aforementioned groups, *n* is the total number of sensors (6 when *j* is S, 10 when *j* is B or 16 when j is SB) and $c_{x,i,j}$ and $c_{y,i,j}$ are the weighing factors for each sensor in longitudinal and translational directions respectively. $c_{x,i,j}$ and $c_{y,i,j}$ are calibrated during first driving maneuvers with a best fitting algorithm with the longitudinal acc_x and transversal acc_y accelerations respectively. After the weighting factors $c_{x,i,j}$ and $c_{y,i,j}$ are defined, $PC_{x,j}$ and $PC_{y,j}$ move according to acc_x and acc_y. An example of the individual row signals of FSRs over time is shown in Fig. 2a, while the processed FSRs as A_B and $PC_{y,B}$ are shown in Fig.2b. In this example the vehicle is parked, engine on, with the driver steady in the correct driving position, with hands on wheel. The computed average A_B and pressure center $PC_{y,B}$ are clearly more reliable than the 16 signals and A_B even perceives the driver breathing.

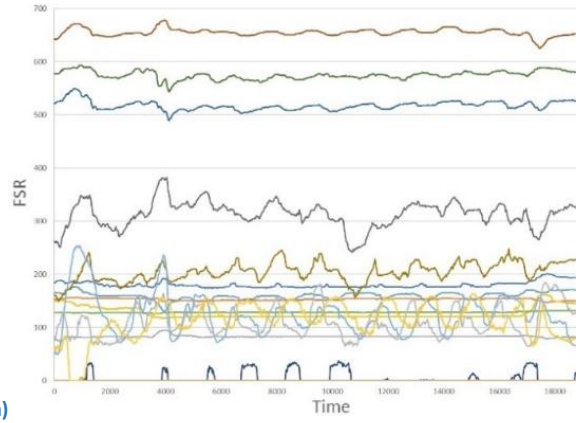

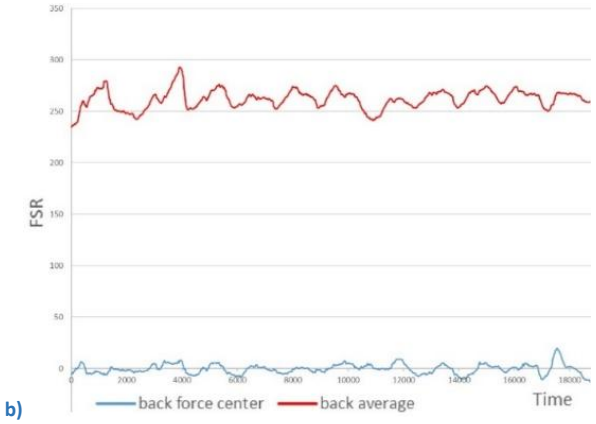

b)

Figure 2. Example of monitoring of a) row signals and b) Average pressure on the Backrest and Pressure Center on the Backrest along transversal direction [Vergnano 2020b].

Three Average criteria - A_S, A_B and A_{SB} - along with four Pressure Center criteria - $PC_{y,S}$, $PC_{y,B}$, $PC_{y,SB}$ and $PC_{x,SB}$ - were identified as significant. These criteria are continuously computed by the controller and compared with the car accelerations acc_x and acc_y. The controller is designed to continuously communicate whether the occupant is in a correct position (OP=0) or if he or she is forward reclined against the steering wheel (OP=1), left reclined against the side door (OP=2), right reclined toward the side seat (OP=3) being distracted by other devices or objects.
All details about the construction of the prototype with pressure sensors embedded in the vehicle seat can be found in [Vergnano 2019a; Vergnano 2020b].

3.2 *High-Resolution Pressure Mat for Monitoring the Pressure Distribution*

This second prototype features a flexible mat designed to cover the surface of the interface being monitored. It can eventually be integrated as a layer within the seat upholstery.
The pressure mat assembly consists of three superimposed layers. Each outer layer consists of parallel copper strips: the lower layer is arranged in rows, while the upper layer is arranged in columns, as shown in Fig. 3a and 3b. The middle layer is a Velostat sheet [Adafruit 2024], a flexible, conductive, and pressure-sensitive material that reduces its electrical resistance when compressed. The matrix measures 600 mm × 500 mm overall and incorporates 750 sensorized cells since it is composed of 30×25 strips, each 20 mm × 20 mm in size. Data scanning and communication to a laptop through a serial port are managed by an Arduino Mega 2560 microcontroller [Arduino 2024]. The scanning process involves sequentially powering each of the 25 Digital Outputs (DOs) at 5V and reading the 30 Analog Inputs (AIs) within the 0–5V range for each powered DO.

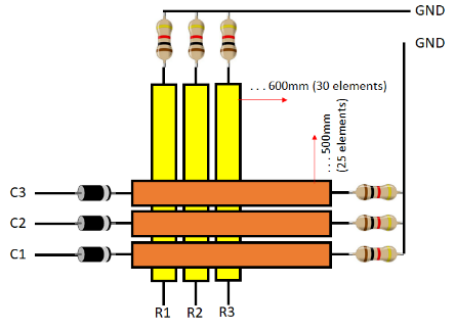

a)

b)

c)

Figure 3. Pressure mat prototype: a) sensor matrix concept with b) copper strips on the outer layers and c) installation on the seat [Vergnano 2019b].

Two individual pads are employed, one for the seat bottom and the other for the seat back, resulting in a total of 1500 sensorized cells, as shown in Fig. 3c. All details about the construction of the high-resolution pressure mat can be found in [Vergnano 2019b].

3.3 *Modular Seat with Separate Regions of Interest*

The third seat is designed with a modular architecture, where each module represents a significant region for detecting interactions between the occupant and the seat [Ng 1995]. The seat comprises 13 modules, as illustrated in Fig. 4a:
1 and 2. Leg areas: the front part of the pan, where the legs rest or provide balance during driving maneuvers;
3 and 4. Sacral area: the rear part of the pan, supporting the majority of the load;
5 and 6. Lower side: the inclined cushions of the pan serving a containment function;
7 and 8. Lumbar area: the lower portion of the backrest, bearing the weight of the back of the occupant;
9 and 10. Back area: the upper section of the backrest, providing shoulder support;
11 and 12. Upper side: the inclined cushions of the backrest for additional containment;
13. Headrest: positioned to support the neck and head, though not always used by the occupant.
Within each module of the seat, the load applied to the padding is transferred to the upper structure, which consists of a 3 mm PVC plate supported by four load cells, as shown in Fig. 4b. These square load cells measure 34×34×8 mm, each with a payload capacity of 50 kg, resulting in a total payload of 200 kg per module. This capacity ensures safe experimental conditions without approaching the load limit. The load cells are mounted on a lower plate designed to allow free flexing through an underlying slot. The four-cell configuration enables electronic connections using a Wheatstone bridge for power and ground wiring to the Arduino Mega 2560 microcontroller [Arduino 2024]. The modular car seat is wired to utilize 13 AIs of the microcontroller. The installed prototype is shown in Fig. 4c.

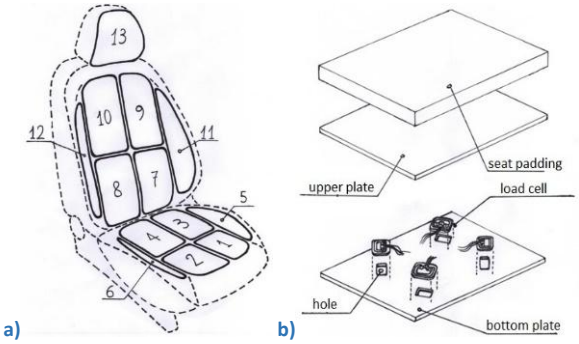

a) b)

c)

Figure 4. Modular seat a) layout, b) construction and c) feasibility prototype [Vergnano 2020a].

All details about the construction of the prototype of the modular seat can be found in [Vergnano 2019c ; Vergnano 2020a].

3.4 Seat with sensors in the lower frame supports

The latest prototype incorporates sensors into a seat designed to closely resemble a roadworthy model, ensuring the preservation of its functionality and comfort. For this research, a driver seat from a 2016 Peugeot 308 SW is repurposed, with only the four seat supports being modified to incorporate a load cell in each. Four DYZ-101–500 kg load cells [DYLoadCell 2024] are installed in the seat supports, as illustrated in Fig. 5 a) and b), to measure the position of the Center of Gravity (CG) of the seat-occupant system. The DYZ-101 is a pancake-type load cell with a compact height and capable of detecting both compression and traction while effectively compensating for off-axis forces. The load cell can withstand a load of up to 500 kg with a safe overload of 150% and a maximum overload of 200%, making it suitable for load measurements in all driving conditions.

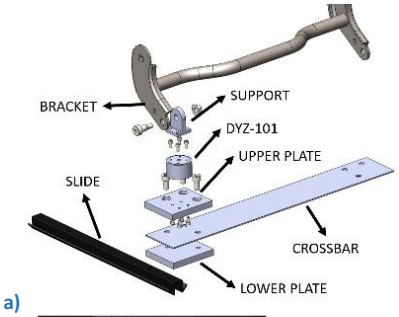

a)

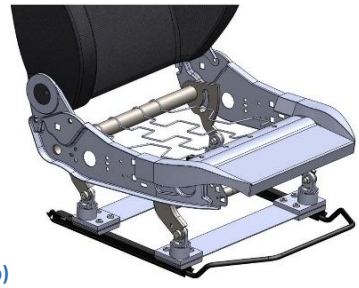

b)

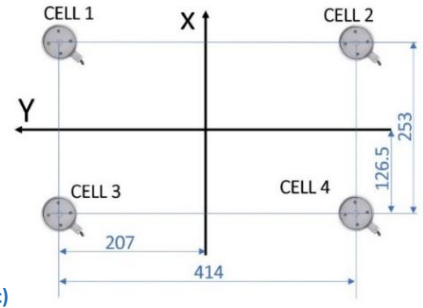

c)

Figure 5. Layout of the last seat prototype with a) supports equipped with DYZ-101 load cell, b) assembled seat in iso view and c) top view of the coordinate system of the CG in normal position [Vergnano 2024].

Again, the seat is also equipped with a BNO055 IMU for monitoring and compensating for the vehicle accelerations when evaluating the CG shifts. All sensors are managed by an Arduino Mega 2560 microcontroller [Arduino 2024], sending all data to a laptop via serial connection using Microsoft Excel Macro-Enabled Worksheet in Office 16 through the PLX-DAQ application.

A calibration routine is preliminarily run when start driving for each trip. Calibration requires the occupant to sit in a normal position to determine the shift factors for the CG and the scaling factors for accelerations. The CG position in the (x_{CGS}, y_{CGS}) plane [Euro Ncap 2024] is computed as the weighted average of the signals from the four load cells relative to their positions, as shown in Fig. 5 c). Negative shift factors are applied to align the CG to (0,0) on average. The x-shift factor is influenced by the occupant body size and the specific adjustments to the height of the seat pan and angle of the backrest. The y-shift factor is minimally affected by the occupant's asymmetrical positioning.

The accelerations acc_x and acc_y are already monitored aligned on $(0,0)$. Scaling factors for accelerations are applied to amplify the IMU signals to match the magnitudes of the CG positions, to make them comparable. These scaling factors are negative because accelerations and inertia forces naturally have opposite signs.

The four monitored and adjusted values x_{CGS}, y_{CGS}, acc_x and acc_y are processed within the same loop cycle to identify the occupant's position.

All details about the construction of this last seat prototype can be found in [Vergnano 2024].

4 EXPERIMENTS

The described prototypes measure pressure at the seat-occupant interface, providing different field resolutions, reliability, and data processing time. The next section will detail the second and third prototypes, showcasing examples of significant pressure distribution readings. Subsequently, the results from experiments with the first and fourth prototypes will be presented, demonstrating occupant monitoring during dynamic driving scenarios.

4.1 Pressure monitoring at seat-occupant interface

In the following experiments with the second prototype, test occupants are instructed to take a normal driving position with hands on wheel and feet on pedals. After one minute of self-adjustment to find a comfortable posture, the pressure field is scanned. Testers are then asked to take a forward-reclined OP, followed by left- and right-reclined OPs. The pressure field is recorded for each posture.

For brevity, results from a driver of 90 kg weight, 185 cm height, and 36 y aged are shown in Fig. 6. The colour scale ranges from 0 (green) to about 850 (red), with each sensor's full scale being

1024. The results demonstrate a significant, though qualitative, pressure distribution. While calibration could improve pressure monitoring reliability, it is challenging due to the nonlinearity of the piezoelectric material. Nonetheless, the array of 1500 cells provide a high-resolution subdivision of the surface, ensuring smooth transitions between different loaded areas.

The experiment reported in Fig. 6b, performed in the normal driving position, reveals an asymmetric posture by the driver, attributed to the differing actions of the right and left legs on the pedals. Additionally, the pressure mat effectively monitors the pressure exerted on the seat's lateral supports. The experiments reported in Figs. 6d, 6f, and 6h demonstrate that the position can be distinctly identified.

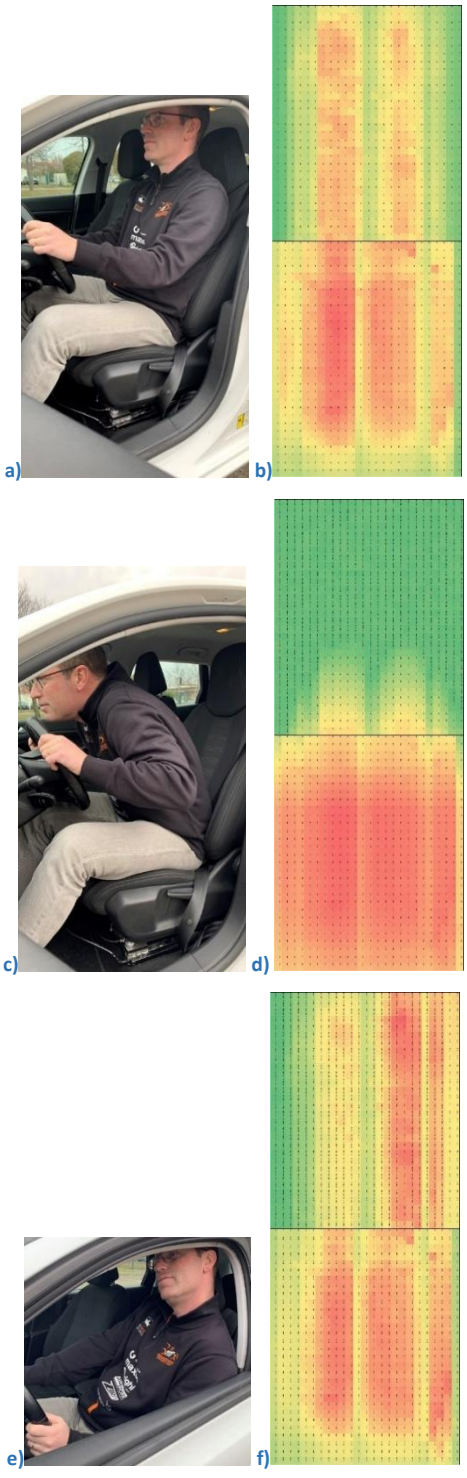

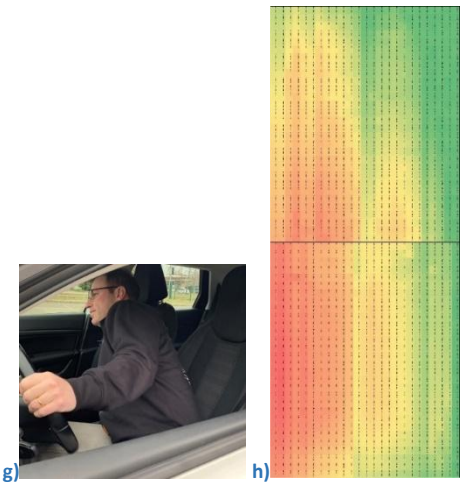

Figure 6. Pressure field as monitored by the pressure mat prototype in the a) and b) normal and in c) to h) the three studied OPs [Vergnano 2019b].

The results in Fig. 6 clearly show that the pressure mat prototype generates a large amount of data, which can be used for advanced activity monitoring and occupant profiling tasks. However, this data must be continuously grouped into significant regions by the control software to identify the OP conditions. To address this, the third prototype is designed for hardware-level grouping by dividing the seat into modules, such as an armchair composed of separate cushions. The system continuously measures and evaluates the force exerted on each module and the vehicle accelerations. In the experiments, the occupant simulates different driving scenarios by adopting different positions on the seat. Fig. 7a shows the occupant in a normal position, naturally distributing his weight across the modules. The OP conditions are clearly identified by the weight distribution, shifting to the front modules (1-2-3-4-5-6) for the forward-reclined OP in Fig. 7b, to the left modules (1-3-5-7-9-11) for the left-reclined OP in Fig. 7c, or to the right modules (2-4-6-8-10-12) for the left-reclined OP in Fig. 7d. Sensor reading with the load cells is much more reliable than the previous prototype and the images effectively report the monitored weight in kg.

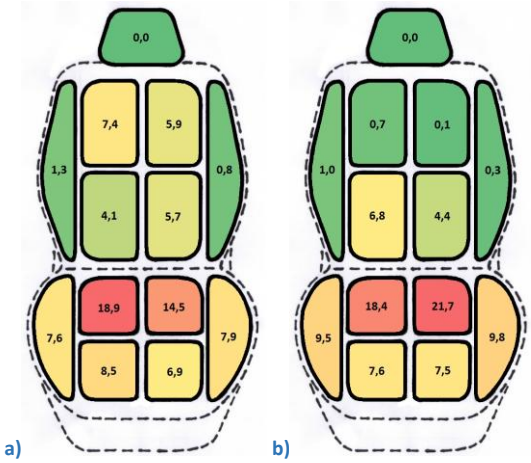

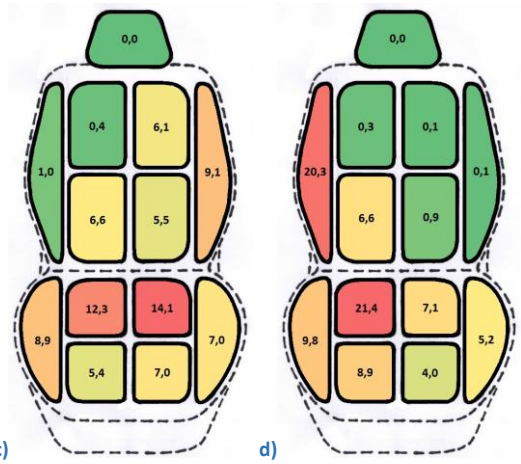

c) d)

Figure 7. Experiments with the modular seat with separate regions of interest in a) normal position, b) forward-reclined OP, c) left-reclined OP and d) right-reclined OP [Vergnano 2020a].

4.2 Occupant position monitoring

Driving experiments with the first prototype with pressure sensors embedded in the vehicle seat were performed at the Autodromo di Modena racing circuit, Italy [Autodromo di Modena 2024]. The vehicle used for testing was a Quattroporte Maserati. The experimental track included a series of maneuvers illustrated in Fig. 8: straight-line acceleration up to approximately 30 km/h speed, counterclockwise 360° turn with a radius of about 10 meters at a constant speed, clockwise 360° turn with the same radius, concluded by straight-line braking.

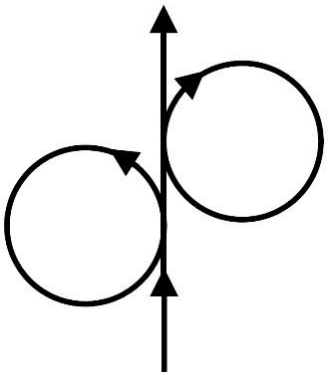

Figure 8. Track for the driving experiments with the first prototype [Vergnano 2020b].

Figure 9 presents the colour map as read by the sensors. The scanned pressure field appears significantly rougher compared to the previous prototypes. However, the detection algorithm in the control software successfully identifies the driver's position for monitoring purposes. Figures 10 to 13 illustrate the position monitoring by comparing Pressure Center and Acceleration for the experiment conducted in the correct driving position and in the forward-reclined, left-reclined, and right-reclined OPs, respectively. In (a) figures $PC_{x,j}$ and acc_x are used to distinguish between correct and OP conditions. Then, in (b) figures $PC_{y,j}$ and acc_y allow to finally identify the specific OP scenario. The sensor readings are derived from voltage signals and are therefore dimensionless. Lastly, the (c) figures display the results of the OP detection routine.

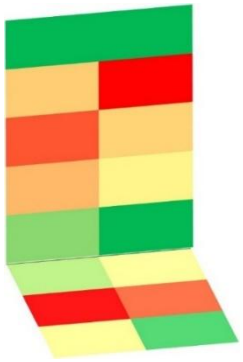

Figure 9. Colours map as read by the 16 sensors of the first prototype.

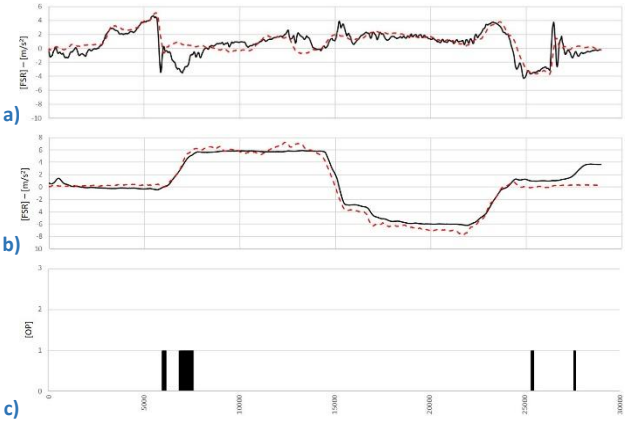

Figure 10. Correct position experiment: (a) acceleration (dotted line) and pressure center (solid) in longitudinal direction for SB sensors group, (b) acceleration and pressure center in transversal direction for S sensors group and (c) OP activation in the system controller [Vergnano 2020b].

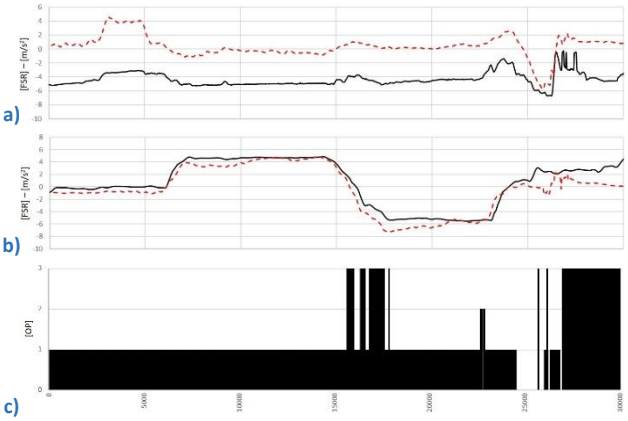

Figure 11. Forward reclined OP experiment: (a) acceleration (dotted line) and pressure center (solid) in longitudinal direction for SB sensors group, (b) acceleration and pressure center in transversal direction for S sensors group and (c) OP activation in the system controller [Vergnano 2020b].

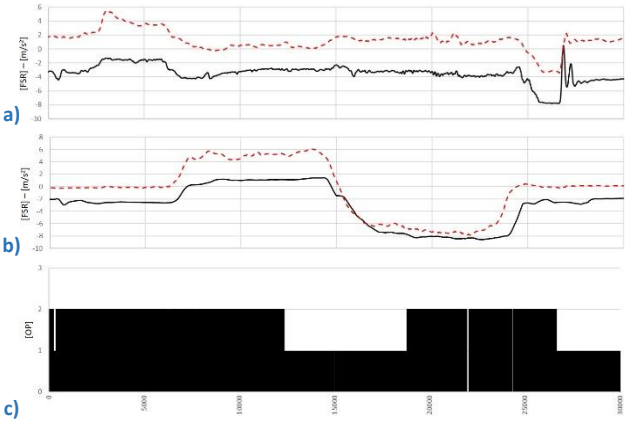

Figure 12. Left reclined OP experiment: (a) acceleration (dotted line) and pressure center (solid) in longitudinal direction for SB sensors group, (b) acceleration and pressure center in transversal direction for S sensors group and (c) OP activation in the system controller [Vergnano 2020b].

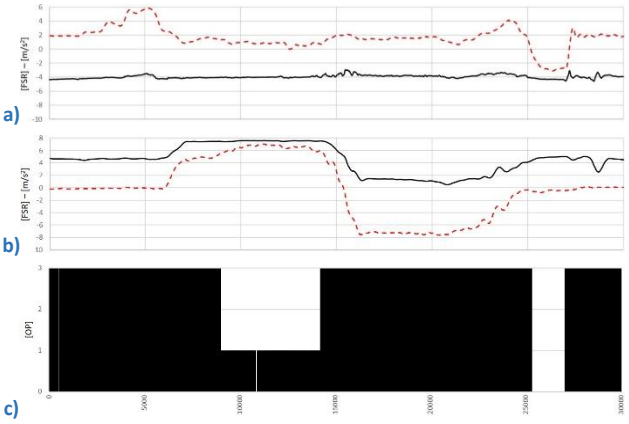

Figure 13. Right reclined OP experiment: (a) acceleration (dotted line) and pressure center (solid) in longitudinal direction for SB sensors group, (b) acceleration and pressure center in transversal direction for S sensors group and (c) OP activation in the system controller [Vergnano 2020b].

$PC_{x,j}$ and $PC_{y,j}$ closely follows acc_x and acc_y respectively under normal driving conditions. In this scenario, the controller detects no OP in 97.1% of the experiment duration. When the driver's back separates from the backrest, the OPs are distinctly identified by comparing $PC_{x,j}$ and acc_x. Then, the comparison of $PC_{y,j}$ with acc_y allows for the identification of specific OP scenarios. The forward-reclined OP is characterized by a longitudinal offset with minimal translational offset. The controller accurately identifies this OP=1 condition during 82.9% of the experiment time. The left-reclined OP is characterized by a negative translational offset, with the OP=2 condition correctly identified in 75.8% of the experiment time. Similarly, the right-reclined OP determines a positive translational offset, and the OP=3 condition is correctly detected in 79.8% of the experiment duration.

Experiments with the fourth prototype with sensors mounted in the lower frame supports were conducted on the runway at the Aero Club of Modena in Italy [Aero Club of Modena 2024]. More extensive experiments were performed due to the fourth prototype's improved reliability and safety. The experiments focused on replicating maneuvers identified as critical for pre-crash and crash conditions [Reed 2021]. The test track, shown in Fig. 14, includes the following sequence: 1) start moving in 1st gear, 2) half-eight turn at approximately 15 km/h speed, 3) maximum acceleration in 2nd gear until speed limit activation at 50 km/h, 4) left lane change, 5) right lane change, 6) hard brake to stop, 7) start moving in 1st gear again, 8) half-eight turn at approximately 15 km/h speed, 9) maximum acceleration in 2nd gear until speed limit activation at 50 km/h, 10) right lane change, 11) left lane change, 12) hard brake to stop.

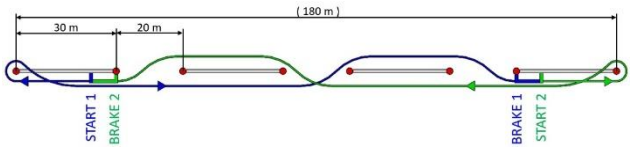

Figure 14. Test track as created on the runway of the Aero Club of Modena [Vergnano 2024].

First, the test driver is asked to adjust the seat to a comfortable position and familiarize himself with the car during a brief driving session. The driver then completes three laps in each of the previously described positions, for a total of 12 laps. The first lap, driven in the normal position, is used to calibrate the device. Each lap lasts approximately 50–55 seconds. The experiments conducted with a driver of 96 kg weight, 185 cm height, and 42 y aged are shown in Fig. 15 for all four positions. In Fig. 15a, the sequence of twelve maneuvers within the lap is further explained, clearly identifiable from the CG movements and car accelerations in longitudinal (red lines) and transverse (blue lines) directions.

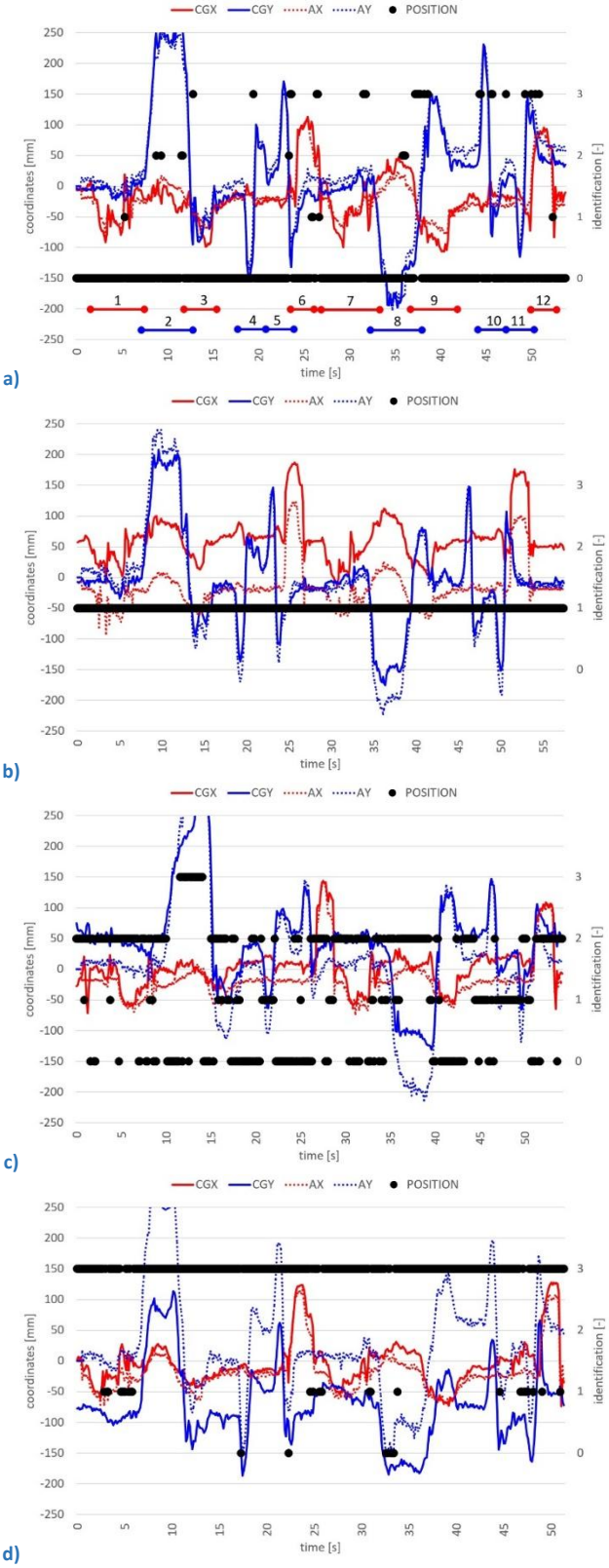

Figure 15. Driver monitoring in real driving tests in a) normal position and in b) forward-reclined, c) left-reclined and right-reclined OPs [Vergnano 2024].

In these extensive experiments, the normal position was correctly identified almost 90% of the time. However, this

undesirable and dangerous outcome needs improvement, as it could compromise the passive safety systems of the car. Misidentifications are mainly caused by very harsh maneuvers, during which the CG is unintentionally shifted from the expected trajectory which replicates the acceleration. This occurs as the driver must hard push on the brake and clutch pedals during braking while also holding up himself by grasping the steering wheel with his hands and leaning against the lower cockpit with his knees. The forward-reclined OP is accurately identified by the controller. The right-reclined OP is correctly recognized approximately 75% of the time. The lower accuracy may be attributed to the driver needing to prioritize maintaining focus on the track for safety reasons during challenging maneuvers in these experiments. Consequently, while the drivers adopted the right-reclined OP, it was not performed to an extreme degree. The left-reclined OP is even harder to identify, with only 50% accuracy. This OP is particularly constrained, as the driver can only slightly recline his body against the door.

Figure 16 illustrates the CG position plots in the (x_{CGS},y_{CGS}) plane for the tests in the normal position (black dots), forward- (red), left- (green), and right-reclined (blue) OPs. The CG positions are adjusted by the scaled vehicle accelerations, so they represent the driver's movements relative to the seat. Each point represents an experimental sample, while the large bordered points represent the average CG positions. Despite deviations caused by harsh maneuvers, the positions can generally be identified through the CG location in the (x_{CGS},y_{CGS}) plane, which represents the vertical projection of the CG position.

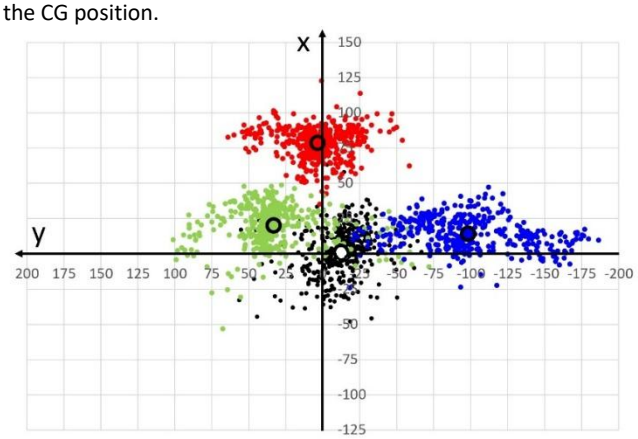

Figure 16. Test track Fig. 18 CG positions reduced by the scaled accelerations for the second test of three, in normal position (black), forward-(red), and left-(green) and right-reclined (blue) OPs, for (a) 1st, (b) 2nd, and (c) 3rd drivers [Vergnano 2024].

5 AIRBAG INTERACTION WITH A TEST DUMMY

This section deals with interaction the between deploying airbag and the dummy or passenger in OP. The test of the driver side dummy sitting close to the steering wheel deploying airbag is presented.

The airbag is triggered by the pyrotechnical initiator, which fires chemical filling producing a high pressure and a high temperature gas. Expansion gas is filtered and cooled. Hybrid systems are equipped with an accumulation chamber with compressed gas. Then the bag chamber is filled by the mixture of the explosion material and composed with the compressed gases tank [Obermann 2004]. Driver-side and passenger-side frontal airbags are activated by the deceleration signal typical for a frontal crash, which is analysed by the vehicle control unit. Misuse activations avoidance is the subject of precise testing.

Lateral and head airbags are activated by the threshold of the lateral acceleration, body deformation of driver chamber pressure in the case of the side crash. The standard and widely accepted crash test dummy for frontal crashes is the Hybrid III dummy of GM production. As the lateral crash test dummies are approved Biosid (GM) and EuroSid (TNO) [Wismans 2020]. The basic requirements for the dummies are anthropometry, simplicity, biofidelity, reproductibility, repeatability, sensitivity, durability (fatigue), and cost. Crash test dummies are equipped with many sensors on which signals are based injury criteria.

Airbag simulation uses finite element methods for the airbag fabric simulation, multibody and finite element methods for dummy dynamics, and thermodynamics for gas flow analysis, as shown in Fig. 17.

Figure 17. Airbag contact with multibody dummy model. [Purš 2017].

The OP test was provided to evaluate the impact of the deploying driver-side airbag against the crash test dummy Manikin situated close to the steering wheel, as shown in Fig. 18. The airbag was activated by the artificial signal on the standing car [First 2012].

Figure 18. Sequence of the OP airbag test [First 2012].

The movement of the dummy head was analysed (blue) and the signal was filtered (orange), as shown in Fig. 19.

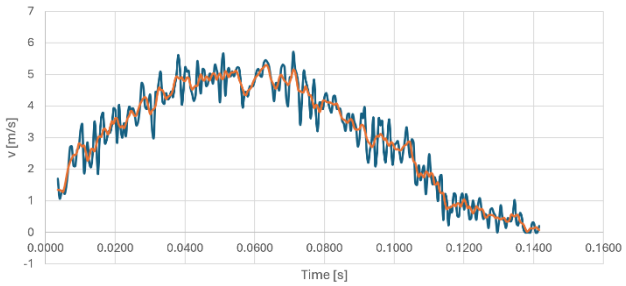

Figure 19. Velocity of the head after airbag impact (courtesy V.Rulc).

The middle value of the head acceleration is about 30 g for the filtered signal with the maximum about 50 g for the filtered signal. If the passenger is exposed to the car-body deceleration during the frontal crash, then the additional reverse impact from the airbag can be critical, especially for the cervical spine and linked soft tissues. Figure 20 presents a principal study of the vertebral and ligament stress distribution (from maximal (red) to zero (blue)) during head hyperextension.

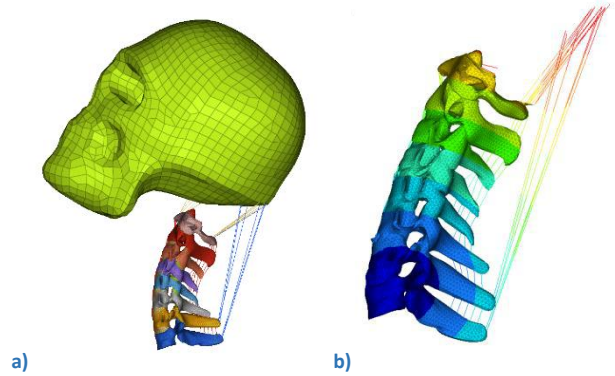

a) b)

Figure 20. Simulation of a) head movement and b) detailed strain results (Purs, 2017).

Basic injuries of the vertebrae are fractures of processes, vertebrae body or the spinal cord disconnection. Most fragile is the dens axis processus and this injury has in many cases serious consequences.

The injury mechanism can lead to the fracture of the spine due to hyperextension with all consequences [Purš 2017]. The maximum stress is detected on the vertebrae C1 and connected ligaments. The vertebrae from C2 to C4 are exposed to high stress, which can lead to the strain injury mechanism of cervical tissues, as shown in Fig. 20.

The airbag tests prove that OP is dangerous in case of the restraint systems (driver side, passenger side, lateral and head airbags) activation. The airbag activation algorithm is based on severity and type of the crash, however warning to the passenger in the case of the OP, increases safety level.

The understanding of mechanisms of injuries, caused by unproper initial condidions like OP, enable the definition of proper control strategy for the addequate restrain effect.

6 CONCLUSIONS

This paper presents how pre-crash scenarios can be identified using sensors embedded in the vehicle seats. Four seat prototypes were presented, along with the results of real driving experiments. The study examines the physical injuries sustained by occupants seated in OP postures. It highlights that the combination of frontal crash inertia loads and the potential impact of airbags on improperly seated occupants can result in overloading of human tissues, especially of the neck spine. The findings highlights the importance of OP detection in preventing severe injuries in such cases. Therefore, future intelligent vehicles should also monitor internal scenarios to be able of implementing adaptive strategies in case of collisions.

REFERENCES

[Adafruit 2024] Adafruit Industries, Pressure-Sensitive Conductive Sheet (Velostat/Linqstat), NY, US, accessed 23 December 2024. Available online: https://www.adafruit.com/product/1361.

[Aero Club of Modena 2024] Aero Club of Modena, Italy, accessed on 23 April 2024. Available online: https://aeroclubmodena.it/ ().

[Arduino 2024] Arduino, Arduino Mega 2560 Rev3, Monza, IY, accessed 23 December 2024. Available online: https://docs.arduino.cc/hardware/mega-2560/

[Autodromo di Modena 2024] Autodromo di Modena, Modena, IT, accessed on 23 December 2024. Available online: http://www.autodromodimodena.it/.

[Bergasa 2006] Bergasa, L.M., Nuevo, J., Sotelo, M.A., Barea, R., Lopez, M.E. Real-time system for monitoring driver vigilance. IEEE Transactions on intelligent transportation systems, 7(1), 63-77, 2006. https://doi.org/10.1109/TITS.2006.869598.

[Borghi 2018] Borghi, G., Fabbri, M., Vezzani, R., Calderara, S., Cucchiara, R. Face-from-depth for head pose estimation on depth images. IEEE transactions on pattern analysis and machine intelligence, 42(3), 596-609, 2018. https://doi.org/10.1109/TPAMI.2018.2885472.

[Bosch 2024] Bosch Sensortec, Smart Sensor BNO055, Reutlingen, DE, accessed on 23 December 2024. Available online: https://www.bosch-sensortec.com/products/smart-sensor-systems/bno055/.

[Chakravarty 2013] Chakravarty, T., Ghose, A., Bhaumik, C., Chowdhury, A. MobiDriveScore—A system for mobile sensor based driving analysis: A risk assessment model for improving one's driving. In: Seventh International Conference on Sensing Technology, Wellington, New Zealand, 338-344, 2013. https://doi.org/10.1109/ICSensT.2013.6727671

[FMVSS 2016a] Standard No. 208, Occupant Crash Protection. Federal Motor Vehicle Safety Standards (FMVSS), Code of Federal Regulations 49-Transportation 6, 2016.

[FMVSS 2016b] Standard No. 214, Side impact protection. Federal Motor Vehicle Safety Standards (FMVSS), Code of Federal Regulations 49-Transportation 6.

[Dong 2010] Dong, Y., Hu, Z., Uchimura, K., Murayama, N. Driver inattention monitoring system for intelligent vehicles: A review. IEEE transactions on intelligent transportation systems, 12(2), 596-614, 2010. https://doi.org/10.1109/TITS.2010.2092770.

[DYLoadCell 2024] DYLoadCell, DYZ-101–500 datasheet, accessed 8 March 2024. Available online: http://www.dyloadcell.com/product/clcgq/82.html.

[Euro Ncap 2024] European New Car Assessment Programme, Euro Ncap Test Protocol—AEB VRU Systems, Version 3.0.3. Accessed on 22 April 2024. Available online: https://cdn.euroncap.com/media/58226/euro-ncap-aeb-vru-test-protocol-v303.pdf.

[EU 2024] European Union, Vehicle General Safety Regulation, Regulation (EU) 2019/2144 of the European Parliament and of the Council of 27 November 2019,

current consolidated version: 07/07/2024. Available online: http://data.europa.eu/eli/reg/2019/2144/oj

[Farmer 2007] Farmer, M.E., Jain, A.K. Smart automotive airbags: Occupant classification and tracking. IEEE Transactions on Vehicular Technology, 56(1), 60-80, 2007. https://doi.org/10.1109/TVT.2006.883768.

[Federspiel 2004] Federspiel, L. Sensor mat for a vehicle seat. U.S. Patent No. 6,794,590, 2004.

[First 2012] First, J., Kovanda, J. Crash tests research reports. Czech Technical University, Prague, 2012.

[Gyi 1998] Gyi, D.E., Porter, J.M., Robertson, N.K. Seat pressure measurement technologies: considerations for their evaluation. Applied Ergonomics, 29(2), 85-91, 1998. https://doi.org/10.1016/S0003-6870(97)00036-7.

[Interlink Electronics 2024] Interlink Electronics), FSR 402, Camarillo, US, Accessed 23 December 2024. Available online: https://www.interlinkelectronics.com/fsr-402 (accessed on 23 December 2024).

[Lund 2003] Lund, A.K. Recommended Procedures for Evaluating Occupant Injury Risk from Deploying Airbags. The Side Airbag Out-of-Position Injury Technical Working Group. Alliance, AIAM, AORC, and IIHS, 2003.

[Maxeiner 1997] Maxeiner, H., Micheal, H. Airbag-induced lethal cervical trauma. Journal of Trauma and Acute Care Surgery, 42.6, 1148-1151, 1997. https://doi.org/10.1097/00005373-199706000-00029.

[Mon 2007] Mon, Y.J. Airbag controller designed by adaptive-network-based fuzzy inference system (ANFIS). Fuzzy Sets and Systems, 158(24), 2706-2714, 2007. https://doi.org/10.1016/j.fss.2007.06.005.

[Ng 1995] Ng, D., Cassar, T., Gross, C.M. Evaluation of an intelligent seat system. Applied Ergonomics, 26 (2), 109-116, 1995. https://doi.org/10.1016/0003-6870(95)00006-X.

[Obermann 2004] Obermann, J., Kovanda, J. Advanced Sensing and Control of Vehicle Airbag Systems. Conference Transportation Sciences, Czech Technical University, Prague, 2004.

[Potula 2012] Potula, S.R., Solanki, K.N., Oglesby, D.L., Tschopp, M.A., Bhatia, M.A. Investigating occupant safety through simulating the interaction between side curtain airbag deployment and an out-of-position occupant. Accident Analysis & Prevention, 49, 392-403, 2012. https://doi.org/10.1016/j.aap.2012.03.007.

[Purš 2017] Purš, H. Injury Mechanisms of the Extreme Load. Dissertation Faculty of Physical Education and Sport, Charles University, Prague, 2017.

[Reed 2021] Reed, M.P., Ebert, S.M., Jones, M.H., Park, B.K.D. Occupant dynamics during crash avoidance maneuvers (No. DOT HS 812 997), Department of Transportation, National Highway Traffic Safety Administration, USA, 2021, accessed on 6 May 2024. Available online: https://rosap.ntl.bts.gov/view/dot/54737.

[SAE 2014] SAE On-Road Automated Vehicle Standards Committee. Taxonomy and definitions for terms related to on-road motor vehicle automated driving systems. SAE Standard J 3016, 1-16, 2014. https://www.sae.org/standards/content/j3016_201401/.

[Schousek 1995] Schousek, T.J. Vehicle occupant restraint with seat pressure sensor. U.S. Patent No. 5,474,327, 1995.

[JASIC 2021] Society of Automotive Engineers of Japan, The automobile and technical regulations, accessed on 26 April 2024. Available online: https://www.jsae.or.jp/files_publish/page/1218/en_vol75_8-2.pdf

[Talarico 2012] Talarico, M. Passive Safety and Crashworthiness. Research report, Czech Technical University, Prague, 2012.

[Vergnano 2019a] Vergnano, A., Leali, F. Out of Position Driver Monitoring from Seat Pressure in Dynamic Maneuvers. In: 2nd International Conference on Intelligent Human Systems Integration: Integrating People and Intelligent Systems (IHSI 2019), San Diego, USA, February 7-10, 2019. https://doi.org/10.1007/978-3-030-11051-2_12.

[Vergnano 2019b] Vergnano, A., Muscio, A., Leali, F. Sensor matrix robustness for monitoring the interface pressure between car driver and seat. In: 2nd International Conference on Human Systems Engineering and Design: Future Trends and Applications (IHSED 2019), Munich, Germany September 16-18, 2019. https://doi.org/10.1007/978-3-030-27928-8_35.

[Vergnano 2019c] Vergnano, A., Piras, A., Leali, F. Vehicle Seat with Occupant Detection System. University of Modena and Reggio Emilia, 26 November 2019. IT Patent No. 102019000022221.

[Vergnano 2020a] Vergnano, A., Piras, A., Leali, F. Modular Car Seat for Monitoring the Pressure Distribution on Regions of Pan and Backrest. In: Proceedings of the 3rd International Conference on Human Systems Engineering and Design, Pula, Croatia, 22–24 September 2020. https://doi.org/10.1007/978-3-030-58282-1.

[Vergnano 2020b] Vergnano, A., Leali, F. A methodology for out of position occupant identification from pressure sensors embedded in a vehicle seat. Human-Intelligent Systems Integration, 2(1), 35-44 2020. https://doi.org/10.1007/s42454-020-00008-w

[Vergnano 2024] Vergnano, A., Giorgianni, C., Leali, F. Monitoring the Center of Gravity of a Vehicle Seat to Detect the Occupant Position, Designs, 8(3), 44, 2024. https://doi.org/10.3390/designs8030044.

[Vlahogianni 2017] Vlahogianni, E.I., Barmpounakis, E.N. Driving analytics using smartphones: Algorithms, comparisons and challenges. Transportation Research Part C: Emerging Technologies, 79, 196-206, 2017. https://doi.org/10.1016/j.trc.2017.03.014

[Wismans 2020] Wismans, J. Reflection on 50 Years of Human Body Modelling and Future Challenges from a Global Perspective. 8th International Symposium Human Modeling and Simulation in Automotive Engineering, Wiesbaden, Germany, 2020.

[White 1991] White, C.W., Behr, L.W. Passenger out-of-position sensor. U.S. Patent No. 5,071,160, 1991.

[Yang 1996] Yang, J., Håland, Y. Modeling of adaptive passenger airbag systems in car frontal crashes. In Proceedings: International Technical Conference on the Enhanced Safety of Vehicles, Melbourne, 1996, 486-501.

[Yaniger 1991] Yaniger, S.I. Force sensing resistors™: A review of the technology. In: Electro International Conference, New York, 666-668, 1991. https://doi.org/10.1109/ELECTR.1991.718294.

[Yoganandan 2007] Yoganandan, N., Pintar, F.A., Zhang, J., Gennarelli, T.A. Lateral impact injuries with side

airbag deployments—a descriptive study. Accident Analysis & Prevention, 39(1), 22-27, 2007. https://doi.org/10.1016/j.aap.2006.05.014.

CONTACTS:

Alberto Vergnano, Associate Professor
University of Modena and Reggio Emilia
Enzo Ferrari Department of Engineering
Via P. Vivarelli, 10
41125 Modena, Italy
+39 059 205 6193, alberto.vergnano@unimore.it, https://www.ingmo.unimore.it/it

Jan Kovanda, Full Professor
University of West Bohemia
Faculty of Mechanical Engineerig
Regional Technological Institute
Univerzitni 8
30100 Plzen, Czech Republic